Article

Not peer-reviewed version

Pegylated Carboxylic Graphene Oxide for Controlled Paclitaxel Delivery to Tumor Cells: In Vitro Evaluation and Cell Studies

Athina Angelopoulou *, Myria Papachristodoulou, Efstathia Voulgari, Andreas Mouikis, Panagiota Zygouri, Dimitrios P Gournis, Konstantinos Avgoustakis *

Posted Date: 18 October 2024

doi: 10.20944/preprints202410.1492.v1

Keywords: graphene oxide; paclitaxel; pegylation; cytotoxicity; programmed cell death

Article

Pegylated Carboxylic Graphene Oxide for Controlled Paclitaxel Delivery to Tumor cells: In Vitro Evaluation and Cell Studies

Athina Angelopoulou [1,*], Myria Papachristodoulou [1], Efstathia Voulgari [1], Andreas Mouikis [1], Panagiota Zygouri [2], Dimitrios P. Gournis [3,4] and Konstantinos Avgoustakis [1,*]

[1] Department of Pharmacy, Medical School, University of Patras, 26500 Patras, Greece; myriapapachri@gmail.com (M.P.); efivoulgari48@gmail.com (E.V.); efivoulgari48@gmail.com (E.V.); andreas27997@gmail.com (A.M.)
[2] Department of Materials Science and Engineering, University of Ioannina, 45110 Ioannina, Greece; pzygouri@gmail.com
[3] School of Chemical and Environmental Engineering, Technical University of Crete, 73100 Chania, Greece; dgournis@tuc.gr
[4] Institute of GeoEnergy, Foundation for Research and Technology-Hellas, 73100 Chania, Greece
* Correspondence: angelopoulou@upatras.gr (A.A.); avgoust@upatras.gr (K.A.); Tel.: 00302610-962317 (K.A.)

Abstract: The functionalization of GO nanomaterials with polyethylene glycol (PEG) polymers has been the most common method to ameliorate stability in physiological media and increase biocompatibility. In this work, carboxylated GO (CGO) was functionalized with PEG polymers of different molecular weight (MW) and structure and loaded with the anticancer drug paclitaxel (PCT). An increase in the MW of linear PEG from 2 to 20 kDA decreased the size and tended to increase the ζ-potential of the pegylated CGO nanoparticles (nCGO-PEG) and a branched (4 arm) PEG(10 kDa) provided nanoparticles with significantly lower size and higher ζ-potential compared to a linear PEG(10 kDa). All nCGO-PEG nanoparticle types exhibited good colloidal stability on storage and in PBS and cell culture medium with the exception of the nCGO-PEG functionalized with the relatively low MW PEG of 2 kDa. PCT loading efficiency fell when the MW of PEG was increased or a branched PEG was used. Pegylation decreased significantly the hemolytic potential of nCGO-PEG nanoparticles. Increased PCT release rate was observed at acidic pH 6.0 compared to physiological pH 7.4 for all PCT/nCGO-PEG formulations. Higher cytotoxicity and apoptotic activity of the nanocarrier-entrapped PCT compared to free PCT against the lung adenocarcinoma A549 cell line at longer incubation times was found as at these longer incubation times a high cellular uptake of the PCT/nCGO-PEG nanoparticles were observed. The results justify further investigation of the potential of PCT/nCGO-PEG as antitumor nanomedicine.

Keywords: graphene oxide; paclitaxel; pegylation; cytotoxicity; programmed cell death

1. Introduction

Graphene Oxide (GO) family nanomaterials, including GO, reduced GO (rGO), and carboxylated GO (CGO) have gained increased attention for biomedical applications, especially in the fields of drug delivery and theranostics [1–4]. The innate, hydrophobic properties of the pristine graphitic lattice of GO nanomaterials raise biosafety and poor biological stability issues, which limit their prospects for biomedical applications. To overcome such limitations, the surface functionalization of GO nanomaterials is being followed either by conjugation chemistry or through exploitation of non-covalent interactions [3,5]. Thus, in order to increase biocompatibility and diminish safety concerns GO nanomaterials have been functionalized with hydrophilic and biocompatible molecules, such as poly(ethylene glycol) (PEG) linear and branched polymers [6,7], dextran [8], bovine serum albumin (BSA) [7], heparin [9], chitosan [10] and polyacrylic acid [11]. GO disperses easily in water but precipitate in saline and physiological media. The colloidal stability of GO nanomaterials in physiological media is enhanced by the covalent attachment of hydrophilic

 doi:10.20944/preprints202410.1492.v1

polymers, such as PEG [12], poly(lacide)-poly(ethylene glycol) copolymers [13] dextran [14], pluronics [15] and tocopherol polyethylene glycol 1000 succinate (TPGS) [16].

Among the various conjugation processes the most widely applied for the functionalization of GO nanomaterials have been the formation of amide linkages by EDC/NHS chemistry, the thiol linkages through dopamine, and the direct polymerization via linkages of initiators on the oxygen functional groups [3,5]. Such conjugation processes are used for the loading of drugs and small molecules, genes, antibodies, and aptamers on GO nanomaterials [4]. The non-covalent modifications include hydrophobic, electrostatic, hydrogen-bonding and π-π stacking interactions [3–5]. Such interactions have made significant contributions on the adsorption of proteins and hydrophobic drugs, providing stabilization of the GO, rGO and CGO and protection from proteolytic degradation of the delivered molecules. The gain obtained from covalent and non-covalent functionalization of GO, rGO and CGO is enhanced biocompatibility and hemocompatibility, increased blood residence time, and elevated deep tumor accumulation [3–5].

Recently, GO family nanomaterials are intensively investigated as drug delivery systems (DDS) in combination with tumor targeting peptides and folic acid (FA) molecules [17,18], metal and metal oxide nanoparticles [19,20], aptamers [20,21] and in combination therapies, such as photothermal/photodynamic therapy and hyperthermia [22], to overcome drug resistance and improve anticancer efficacy. Li et al. [17], combined the effect of HN-1 (TSPLNIHNGQKL) tumor-targeting peptide and doxorubicin with nano GO that was covalently functionalized with diamino-PEG (NH_2-PEG4000Da-NH_2). The drug doxorubicin (DOX) was loaded through π-π stacking and hydrogen bond interactions with the PEG modified nano GO. The formulation was evaluated for its HN-1 targeting effect against oral squamous cell carcinoma (OSCC) in CAL-27 and SCC-25 cell lines, showing significant internalization and increased anticancer effect (DOX cytotoxicity). In another study by Vinothini et al. [18], GO was grafted with methyl acrylate (MA) via in situ atom transfer radical polymerization, in order to create biodegradable GO surfaces for the conjugation of FA and the loading of PCT through π-π stacking interactions (GO-g-MA/FA). The targeting ability and cytotoxic effect of the formulations were examined in human MDA-MB-231 breast cancer cells. The in vivo evaluation of the PCT-loaded GO-g-MA/FA formulations in DMBA induced breast cancer rats, revealed their antitumor effect through the inhibition of tumor size and the regulation of mitochondrial mediate apoptotic cascade. The combination of CGO with gold nanoparticles (GNP) was studied by Samadian et al. [19] for the development of a theranostic nanomedicine system. The CGO was functionalized with PEG-amine and thiol-terminated FA for the conjugation of GNP and the loading of DOX. The final system expressed pH-sensitive DOX release and elevated anticancer activity against MCF-7 human breast cancer cells. Hussien et al. [20] investigated the anticancer effect of superparamagnetic GO (MGO) formulations conjugated with MUC1 targeting aptamer and further loaded with PCT. The MGO formulations showed elevated biocompatibility in L-929 human normal fibroblasts. Moreover, the final formulations showed increased binding affinity to MCF-7 cancer cells and significant cytotoxicity. The effect of aptamer on the targeted delivery of CGO was examined by Yaghoubi et al. [10] in human gastric adenocarcinoma AGS cell line. The CGO was functionalized with AS1411 aptamer for the co-delivery of curcumin and DOX. The successful targeting effect of the aptamer resulted in elevated cytotoxicity and the regulation of gene expression related to cell cycle arrest (G1 phase) and apoptosis. GO was, also investigated in thermally-responsive formulations by Jedrzejczak-Silicka et al. [22]. The GO surface was functionalized with hydroxycamptothecin (GO-HCPT) and hyperthermia was induced via application of a rotating magnetic field (RMF). The GO-HCPT nanomaterials exhibited high cytotoxicity against MCF-7 cancer cells and regulated mitochondrial metabolism, resulting in enhance antitumor activity.

Among the various functionalizations used, PEG modification of nanoparticulate drug carriers is the most frequently applied owing to many desirable PEG properties, including variety in functional groups, linear or branched polymeric structure, and molecular weight (MW), that provide flexibility in anticancer drug delivery and cancer theranostics [23–26]. The presence of coating materials, such as PEG, can highly affect the size, shape, colloidal stability, biocompatibility, drug loading and release profile, thus resulting in variations in cellular uptake, biodistribution and

 doi:10.20944/preprints202410.1492.v1

anticancer efficacy. Moreover, the characteristics of the polymeric chain, as MW and linear/branch structure, can further differentiate the surface properties and protein adsorption [23,25]. Thus, in our study the functionalization of CGO with PEG-NH_2 polymers that vary in molecular weight (low and high MW), and polymer structure (linear and 4-arm) was investigated for the development of paclitaxel-loaded CGO nanoformulations. The CGO served as an excellent surface for the covalent modification with PEG-NH_2 and the efficient paclitaxel (PCT) loading through π–π stacking interactions. Higher biocompatibility and efficacy of drugs loaded onto GO-COOH have been shown in previous studies [21,27,28]. Optimum PCT-loaded CGO, based on physicochemical and drug release properties, was investigated for the in vitro anticancer efficacy in the A549 human lung cancer cell line.

2. Materials and Methods

2.1. Materials

Graphite flakes (purum, powder ≤0.2 mm), potassium chloride (purum > 98.0 %), nitric acid (HNO_3 65 % wt) and sulfuric acid (H_2SO_4 95–97 % wt) were obtained from Fluka. Monomethoxy poly(ethylene glycol)-amine (mPEG-NH_2 of 2 kDa, 10 kDa, and 20 kDa), 4-armed poly(ethylene glycol)-amine (4-arm PEG-NH_2 of 10kDa), N-ethyl-N'-(3-dimethyl aminopropyl) carbodiimide hydrochloride (EDC-HCl, >98 %, MW: 191.7 g/mol), N-hydroxysuccinimide (NHS, >98%, MW: 115.09 g/mol), triethylamine (Et_3N, $(C_2H_5)_3N$, >99.5 %) and fluorescein isothiocyanate (FITC, >90% HPLC) were obtained from Sigma-Aldrich. Paclitaxel was purchased from LC Laboratories, USA. All other chemicals and solvents were of analytical grade.

2.2. Synthesis of Carboxylated Graphene Oxide

The oxidation of graphite for the synthesis of graphene oxide (GO) and further preparation of carboxylated graphene oxide (CGO) was followed and characterized as reported previously in Spyrou et al. [29] and Zygouri et al. [30]. Details for the successful synthesis and characterization of GO and CGO are reported in Supplementary Information (SI).

2.3. Nano Carboxylated Graphene Oxide (nCGO) Particles

Nanoparticles of CGO (nCGO) were prepared in aqueous suspensions. An initial concentration of 3 mg CGO was dispersed in 5 ml D-H_2O through bath sonication (50 kHz, 350 W) for 2 hours followed by probe sonication (50/60 kHz, 130 W) in an ice-bath for additional 3 hours. The obtained CGO aqueous dispersion was centrifuged at 12000 g for 30 min and filtered through Millipore filters of 0.2 μm diameter, to provide nCGO particles. The nCGO yield measured by freeze-drying samples and weighing the solid residues was 54 % wt.

Then, amino-terminated poly(ethylene glycol) (PEG-NH_2) polymers of varied molecular weights were utilized for the preparation of surface pegylated nCGO dispersions. EDC/NHS chemistry was used for the amide conjugation of PEG-NH_2 with the activated free carboxyl groups of the nCGO, as in previous studies [32]. Thus, equimolar concentrations of 0.002 mmol mPEG-NH_2 (2 kDa, 10 kDa, and 20 kDa) and 4-arm PEG-NH_2 (10 kDa) were dissolved in 500 μl D-H_2O and added dropwise in the nCGO dispersion under bath sonication for 5 min. Then, equimolar concentrations of 0.015 mmol EDC-HCl / NHS dissolved in 200 μl D-H_2O were added dropwise. The pH of the reaction solution was adjusted to 8 with Et_3N, so that the amino groups remain deprotonated and react with the carboxylic acid groups. The reaction mixture was bath-sonicated in ice-bath for 30 min and then gently stirred for 24 hours at ambient temperature in the dark. The reaction product was purified by extended dialysis against water in the dark. Dialysis membranes of appropriate MWCO (14 kDa and 50 kDa) were used depending on the MW of the PEG-NH_2 polymers. Then, the purified product was centrifuged at 12000 g for 30 min and filtered through Millipore filters of 1.2 μm diameter. The yield of the nCGO-PEG conjugates was in the range 14-32 % wt depending on the MW of the mPEG-NH_2 polymers.

The nCGO-PEG(10kDa) particles were fluorescent labelled with FITC that was conjugated through EDC chemistry. For the reaction process, 0.5 mg/ml nCGO-PEG were used and 0.5 mg EDC were added dropwise. The reaction mixture was sonicated in ice-bath for 1 hour for the activation of

 doi:10.20944/preprints202410.1492.v1

the carboxylic acid groups. Then, 100 μl FITC from a stock solution (1mg/ml in D-H_2O) were added dropwise and the pH was adjusted to 8 with Et_3N. Following, the mixture was gently stirred at ambient temperature for 24 hours in the dark. The final product was purified by extended dialysis against D-H_2O. The purified nanoCGO-PEG/FITC was stored in the fridge (4 °C) until further use.

The composition of the nCGO-PEG particles was examined by Thermal gravimetric analysis (TGA) on a TA Instrument Q500 series Thermogravimetric Analyzer at a heating rate of 10 °C/min from room temperature to 600 °C in N_2. The nCGO-PEG conjugates were characterized by Fourier transform infrared spectra (FT-IR) obtained from 600 to 4000 cm-1 using a DigiLab Excalibur series FTS 3000 spectrometer equipped with an attenuated total reflectance (ATR) and a class II laser. The morphology of the nCGO-PEG particles was characterized by transmission electron microscopy (TEM) using a JEOL JEM-2100 microscope at an acceleration potential of 200 kV, equipped with a GATAN camera Erlangshen ES500W, model 782. Specimens for TEM were prepared by spreading an aqueous solution of 0.1 mg/ml concentration onto a carbon coated cooper MS200 grid, which was air dried before observation.

The colloidal stability of the nCGO-PEG particles was assessed by storing samples of the particles at room temperature (20 °C) for up to 4 weeks and by incubating the samples in mildly agitated PBS and RPMI 1640 cell medium (50 %v/v dilution) at 37 °C for 5, 24 and 48 hours. The ζ-potential and average hydrodynamic size were recorder in a ZetaSizer Nano series Nano-ZS (Malvern Instruments Ltd, Malvern, UK) equipped with a He-Ne Laser beam at a wavelength of 633 nm and a fixed backscattering angle of 173° was used.

The biocompatibility of the nCGO and nCGO-PEG particles was assessed by hemolysis assay, as previously described [33]. Blood samples from healthy donors (obtained from University Hospital of Patras, Greece) were collected in heparin tubes and centrifuged at 1000 g for 5 min for plasma separation. The red blood cells (RBC, erythrocytes) were washed thrice with normal saline and a ratio of 1:20 pure RBC was prepared at a final volume of 2 ml. The nCGO and nCGO-PEG particles were prepared in PBS for concentrations in the range of 0.5 μg/ml to 1000 μg/ml. Then, equal quantities of RBC and particles were mixed with a rotor shaker, incubated at 37 °C for 4 hours and were gently agitated every 30 min. Next, the samples were centrifuged at 1000 g for 5 min. The supernatant containing the hemoglobin was transferred in 96-well plates and the absorbance was measured at 570 nm using a MPR-700 Plate Reader, Biotech Engineering Management Co. Ltd (UK). For positive and negative controls, PBCs were exposed to 10 % Triton X-100 solution (+, positive, 100% hemolysis) and PBS (-, negative, 0% hemolysis), respectively at identical conditions. The test was repeated thrice and the percent of hemolysis was calculated from the following equations

$$\boldsymbol{Hemolysis}\ \% = \frac{A_{nCGO} - A_{negative}}{A_{positive} - A_{negative}} \times \mathbf{100} \quad (1)$$

where, A_{nCGO}, $A_{positive}$ and $A_{negative}$ are the absorbance of hemoglobin contained in the supernatant of the nCGO and nCGO-PEG particles, in the negative control and in the positive control, respectively.

2.4. Paclitaxel Loading and Release from nCGO-PEG Particles

For the drug loading process, a paclitaxel (PCT) solution (1 mg/250 μl methanol) was added dropwise in 500 μl of nCGO-PEG dispersions. The reaction mixture was bath sonicated for 15 min and gently agitated for 24 hours, in the dark. Then, the reaction mixture was dialyzed against excess D-H_2O for 24 hours in a dialysis membrane (MWCO 12kDa) in order to remove the organic solvent and non-entrapped PCT. Drug loading was measured by UV-Vis spectroscopy, in a UV-1800 Shimadzu spectrophotometer. The nCGO-PEG/PCT particles were analyzed at 227 nm [34], with the absorbance of blank (no drug) nCGO-PEG particles being extracted upon measurement. PCT quantification was assessed based on a calibration curve with R^2 = 0.9976 and limit of quantification 0.01 μg/ml with the linear part of the standard curve used from 0.01 to 100 μg/ml. The dispersion solution for PCT quantification was D-H_2O:MeOH = 60:40 in %v/v. The PCT loading capacity was calculated according to the following formula:

 doi:10.20944/preprints202410.1492.v1

$$LC\ \% = \frac{W}{W_C + W} \times 100 \quad (2)$$

where W, W_C were the amount of loaded PCT according to the UV-Vis spectroscopy, and the amount of nCGO-PEG particles, respectively.

The release profile of PCT from the nCGO-PEG/PCT particles was obtained under sink conditions in 1xPBS buffer pH 7.4 and 6.0. In brief, nCGO-PEG/PCT samples were enclosed in dialysis membranes (MWCO 12 kDa) and transferred to vials containing 20 ml PBS. The vials were put in mildly agitated water bath (37 °C). At predetermined time intervals (30 min, 1, 2, 4, 6, 12, 24, 48 hours), the release medium was completely removed and replaced with fresh PBS at 37 °C. The release medium was treated with 2 ml of DCM (Dichloromethane) for the extraction of the released PCT. The extraction process was repeated in triplicate for each sample. Then, DCM containing the released PCT was collected, allowed to evaporate at room temperature in a fume hood, and the solid residue was dissolved in 1 ml of D-H_2O:MeOH = 60:40 (%v/v). The obtained solutions were assayed for PCT by UV-Vis spectroscopy at 227 nm, as described above.

2.5. Cellular Evaluation of the nCGO/PEG Particles

The human A549 (ATCC) lung adenocarcinoma epithelial cells were cultured under standard conditions [33]. The anticancer activity of nCGO-PEG/PCT particles against the A549 cells was assessed using the propidium iodide (PI) fluorescence method [32]. The cells were seeded in 24-well plates ($5x10^4$ cells per well) and proliferated for 24 hours (37 °C in a humidified atm. with 5 % CO_2). Then, the cells were treated with PCT and nCGO-PEG/PCT particles at indicated concentrations (0, 1, 5, 10, 17, 25 μg/ml of drug) for varied time periods of 5, 24, and 48 hours. The blank nCGO-PEG (no drug) and nCGO (no PEG, no drug) particles were also evaluated as controls at similar concentrations to the drug-loaded ones. The cells were then washed with PBS and harvested (0.25 %w/v trypsin) and transferred to FACS tubes for centrifugation (1600 rpm for 5 min). Then, cells were stained with PBS containing 5 μl PI (1 mg/ml PI stock solution) for 1 min. The cell death distribution was determined via flow cytometry analysis (for PI fluorescence with $\lambda_{exc.}$ = 488 nm, $\lambda_{em.}$ = 620 nm) in a FACS Calibur, Coulter Epics XL-MCL apparatus. As a negative control unlabeled cells were used to calculate the background fluorescence of the cells. Data analysis was performed with the WinMDI cytometry analysis software.

For the cellular uptake experiments, nCGO and nCGO-PEG particles were labelled with FITC. The A549 cells were treated with 10 μg/ml nCGO-PEG/FITC and nCGO-FITC samples for varied time periods (1, 5, 24 and 48 hours). The cells were grown in monolayers and then harvested and washed with PBS. The cellular uptake was quantitatively evaluated by flow cytometry (FITC fluorescence $\lambda_{exc.}$ = 488 nm, $\lambda_{em.}$ = 543 nm) in the above FACS Calibur analyzer. The background fluorescence of untreated cells was used as a negative control. The visualization of the cellular uptake was performed following the PI post-fixation staining method proposed by Hezel et al. [35] The PI staining method is normally being used for the quantitative assessment of cell death. In the post-fixation PI method, the cellular fixation with paraformaldehyde and disruption of cellular membrane with Triton X is prior to PI staining. This way, PI is being allowed to diffuse and interact with nuclear and cytoplasmic nucleic acid. Thus, intact non-degenerating cells may be visualized. In the post-fixation staining method, cells were grown in cover slips and treated with 10 μg/ml nCGO-PEG/FITC particles for 24 hours. Then, the cells were washed with PBS, and fixed with 4 %v/v PFA (paraformaldehyde) for 15 min directly on the cover slips. Following, the cells were washed and cellular membrane disruption was promoted by 0.1 %v/v Triton X 100 for 10 min. Finally, the cells were washed with PBS and treated with PI for 15 min. The final specimens were imaged in a Leica Microsystems DMLB I/2001 microscope equipped with a Leica fluorescence source and a Leica DC 300 camera.

In the Cell apoptosis study, the cells were treated with PCT and nCGO-PEG/PCT at 10 μg/ml for 1, 5, 24, and 48 hours. The nCGO-PEG and nCGO particles were used as control. After treatment, the cells were harvested and washed with PBS. Then, cellular apoptosis was determined with the FITC Annexin V Apoptosis staining method according to a standard protocol [33]. In brief, cells were washed with PBS, harvested, and centrifuged in FACS tubes (1600 rpm, 5 min). Then, cells were

 doi:10.20944/preprints202410.1492.v1

washed and re-suspended to 1xAnnexin V binding buffer and centrifuged (1600 rpm, 5 min). Cells were then re-suspended to 100 μl 1xAnnexin V binding buffer with 5 μl FITC Annexin V solution (in the dark, 15 min). Finally, the cells were washed with 1xAnnexin V binding buffer. Apoptosis was analyzed in the above FACS Calibur analyzer (Annexin V fluorescence $\lambda_{exc.}$ = 495 nm, $\lambda_{em.}$ = 519 nm). The background fluorescence of untreated cells was used as a negative control.

2.6. Statistical Analysis

For the statistical analysis of experimental data, appropriate statistical methods (Student's t-test and one-way ANOVA) were applied using the IBM SPSS Statistics 25 software.

3. Results

3.1. Characterization

The successful functionalization of nCGO with PEG-amine was shown with FT-IR, ^{1}H NMR and TGA. In the FTIR spectra of the nCGO-PEG particles (Figure 1A) all the characteristic peaks of nCGO were observed, including the broad band around 3400 cm^{-1} attributed to the stretching vibrations of -OH groups, the peak at 1630 cm^{-1} ascribed to the stretching vibrations of -C=O, the peak at 1386 cm^{-1} denoting the deformation vibrations of the C-OH groups and the band at 1061 cm^{-1} ascribed to the stretching vibrations of the C-O-C. Moreover, the main peaks of PEG polymers were recognized at 2883 cm^{-1} attributed to the stretching vibration, of methylene (-CH_2-) groups, and the peak at 1100 cm^{-1} ascribed to the stretching vibrations of C-O-C groups. The effective conjugation of PEG on nCGO was verified by the following bands in the spectrum of nCGO-PEG which do not exist in the spectrum of nCGO: (a) the band at 1625 cm^{-1} attributed to the stretching vibration of the -C=O- group of amide type I, (b) the band at 1592 cm^{-1} ascribed to the stretching vibration of -NH of amide type II and (c) the band at 2883 cm^{-1} attributed to the stretching vibration, of methylene (-CH_2-) groups of PEG [36–40]. The proton NMR spectra of the nCGO, PEG-amine and nCGO-PEG were recorded in D_2O (Figure S4 of SI). The nCGO and nCGO-PEG spectra exhibited a peak at 2.21 ppm attributed to the nCGO methylene (–CH_2-) protons accompanied with varied weak peaks at the range 1.0 - 2.0 ppm of the aliphatic area attributed to the - CH - CH protons of GO. They also had a low peak at 8.5 ppm which is attributed to the aromatic protons of the graphite lattice [17,41,42]. The peak at 3.69 ppm in the spectrum of PEG-amine and nCGO-PEG is ascribed to the methylene (-CH_2-) protons of PEG.

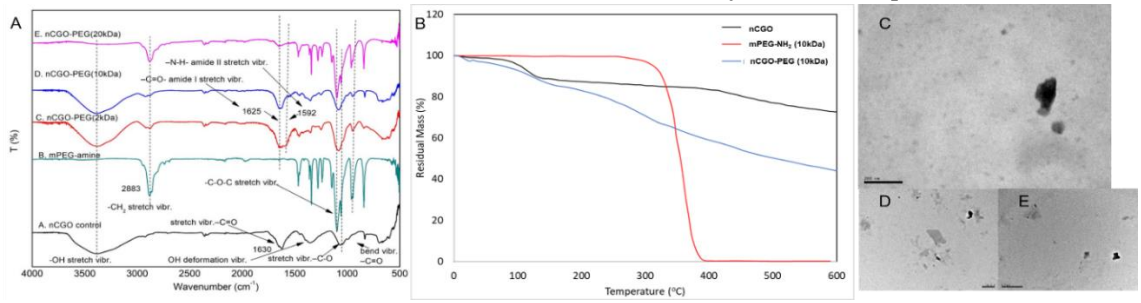

Figure 1. Characterization of nCGO-PEG particles A) FTIR spectra of nCGO (black) mPEG-NH_2 (amine) polymer (light blue), and nCGO-PEG particles of varied MW (2, 10, 20 kDa) (red, blue magenta), B) thermograms of nCGO, mPEG(10 kDa)-NH_2, and nCGO-PEG(10 kDa) up to 600 °C, C) SEM micrographs of nCGO-PEG(10 kDa) at scale bar of 200 nm, 50 nm (D) and 100 nm (E).

The TGA thermograms of the nCGO-PEG particles (Figures 1 and S5 of SI) exhibited mass loss profiles that combined the characteristics of nCGO matrix and PEG polymers and were dependent on the polymers MW. The nCGO exhibited an initial stage of mass loss of about 10 % at 100 -150 °C that can be attributed to the evaporation of adsorbed water. A mass loss of only 8 % was observed at 150 - 400 °C due to high thermal stability of the -COOH complexes. A final third stage of mass loss of around 10 % was observed at 400 - 600 °C, which was due to the decomposition of the carbon skeleton. For PEG polymers complete decomposition was observed at 350 – 420 °C, regardless the MW of the

 doi:10.20944/preprints202410.1492.v1

polymer [13,19]. In order to determine the exact composition of the nCGO-PEG conjugates (proportion of CGO and PEG-NH_2) from the thermograms (Table 1), the equation (1 – M) n = W [13] was used, where M is the polymer percent weight of the composite, n is the percent residual weight of nCGO and W is the percent residual weight of the composite.

Table 1. Characteristics of the nCGO and nCGO-PEG particles of varied PEG MW (2, 10, 20 kDa) and structure (linear, 4-arm).

Sample	Yield (%)	CGO weight ratio (%)	PEG-NH_2 weight ratio (%)	PCT Loading (%)	Average size (nm)	PdI	ζ-Potential (mV)
nCGO	54.89 ± 6.85	-	-	-	76.10 ± 3.49	0.354 ± 0.036	-47.82 ± 2.36
CGO-PEG(2kDa)/PCT	26.85 ± 0.90	23.31	76.69	67.64 ± 1.32	181.4 ± 3.40	0.431 ± 0.051	-30.84 ± 3.36
CGO-PEG(10kDa)/PCT	14.63 ± 2.69	60.84	39.2	52.43 ± 2.38	140.5 ± 1.02	0.311 ± 0.089	-24.78 ± 0.61
CGO-PEG(20kDa)/PCT	32.38 ± 0.85	20.40	79.6	38.88 ± 2.42	104.2 ± 1.16	0.276 ± 0.012	-28.35 ± 5.04
CGO-PEG(4arm 10kDa)/PCT	23.61 ± 1.51	21.95	78	33.66 ± 1.74	110.3 ± 2.37	0.209 ± 0.023	-17.14 ± 2.65

The average hydrodynamic size and ζ-potential of the nCGO and nCGO-PEG particles are presented in Table 1. According to DLS, the average size (hydrodynamic diameter) of nCGO was around 80 nm, while the average size of the nCGO-PEG particles ranged between 100 and 180 nm. The increased size of the nCGO-PEG conjugates was also verified by TEM (Figure 1 and Figure S6 of SI) and was probably due to the presence of the hydrated PEG molecules on the particles and possibly to the slight nanosheets aggregation caused by the reaction between activated carboxyl groups (-COOH) in neighboring nanosheets forming anhydrides [37]. The conjugation of PEG appeared to have an impact on the average size of the nCGO-PEG particles that depended on the MW and structure of PEG. An increase in the MW of the PEG caused a decrease in the size of the particles (Table 1), presumably due to the more effective steric stabilization of the conjugates by the high MW PEG molecules. Also, the four arm PEG appeared more effective steric stabilizer than the one arm PEG, resulting in lower particle size for the nCGO-PEG particles functionalized with the four arm PEG polymer (Table 1).

The ζ-potential of the nCGO was highly negative (- 50 mV) due to the presence of –COOH groups on the lattice. After PEG conjugation, the nCGO-PEG particles exhibited an increase in ζ-potential (lower negative values, Table 1) that depended on the MW of the PEG polymers ranging from -20 mV to -35 mV that further confirmed the successful PEG conjugation on graphene oxide surface [21].

3.2. Colloidal Stability of nCGO-PEG

The results of the colloidal stability study of the nCGO and nCGO-PEG particles are shown in Figures 2 and S7 of SI. The size and ζ potential of the nCGO and nCGO-PEG particles remained essentially constant with storage at ambient temperature for a period of four weeks, indicating good physical stability (Figure S7 of SI). The only exception was the nCGO-PEG(2 kDa) particles which showed an increase of size after a week's time storage, assuming a value around 300 nm, which, however, remained essentially constant for the remaining storage period of time (Figure 2A, B). All nCGO-PEG particles, with the exception of nCGO-PEG(2 kDa) particles, were stable in PBS and only small changes in size and ζ-potential of the particles were observed during the 48 hours incubation period (Figure 2 C,D). The size and ζ-potential of the nCGO-PEG particles tended to increase with incubation time in RPMI 1640 cells culture medium, however no aggregation or sedimentation was observed. Again and in accordance with the storage stability results (Figure 2A), the nCGO-PEG(2 kDa) particles were the less stable particles and tended to aggregate in RPMI 1640 with incubation time, reaching a size of around 500 nm at 48 hours (Figure 2C).

 doi:10.20944/preprints202410.1492.v1

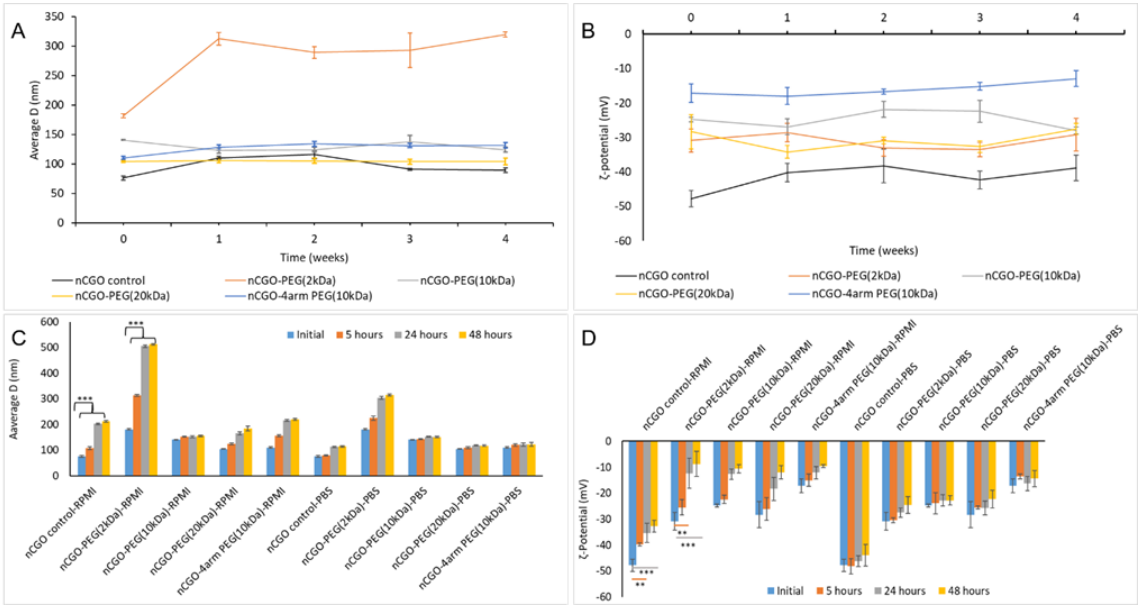

Figure 2. Colloidal stability of the nCGO and nCGO-PEG particles exhibiting A) average size distribution by DLS and B) distribution of ζ-potential for a period of 4 weeks. The stability of nCGO and nCGO-PEG particles in RPMI and PBS media as presented by C) average size and D) ζ-potential at 5, 54, and 48 hours. The statistical significance is ** $p < 0.001$, *** $p < 0.0001$.

3.3. Hemolysis Assay Results

The hemolytic potential of the nCGO and nCGO-PEG particles was determined as an indication of particles biocompatibility. Nanoparticles should not cause hemolysis if they are intended to be applied as drug delivery systems entering the blood stream. The particles were evaluated for their hemolytic activity by the disruption of erythrocytes membrane in human red blood cells (Figure 3). The hemolysis caused by nCGO-PEG was very low, lower than 5 %, even at the high concentration of 1 mg/ml. The pristine nCGO particles caused higher hemolysis than the nCGO-PEG particles, reaching a hemolysis value of around 15 % at the concentration of 1 mg/mL [43].

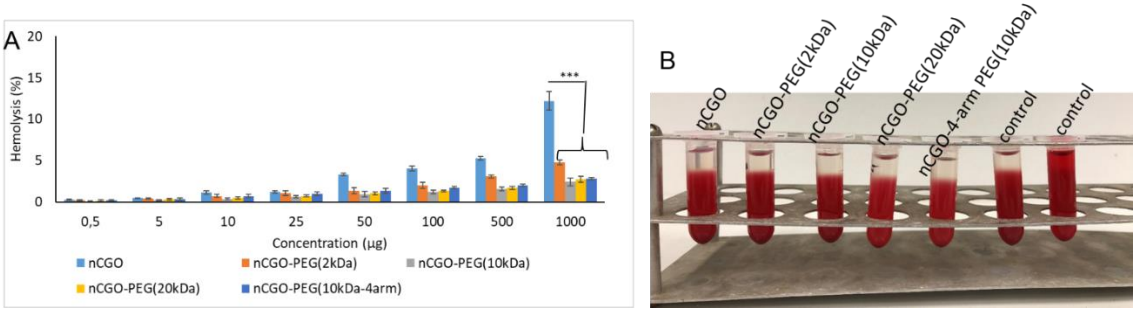

Figure 3. (A) hemocompatibility at human Red Blood Cells (RBC) at varied concentrations of the nCGO and nCGO-PEG particles. (B) representative photographs of nCGO and nCGO-PEG particles for their hemocompatibitily at a concentration of 25 μg/ml and the control (positive, negative) samples. The statistical significance is *** $p < 0.0001$.

3.4. Loading and Release Profiles from nCGO-PEG/PCT Particles

The main interactions facilitating PCT loading on graphene and graphene oxide sheets are via π-π stacking and hydrophobic interactions mainly promoted by the increased binding energy of PCT with both graphene and graphene oxide. Thus, PCT adsorption on graphene and graphene oxide is favorable through the three benzene rings that provide PCT with a strong hydrophobic character in aqueous media [44]. In this study we applied pegylation on CGO nanosheets and it was found that the MW and structure of the conjugated PEG-NH_2 had an impact on the loading capacity of PCT

 doi:10.20944/preprints202410.1492.v1

(Table 1). Among linear PEG-NH_2 conjugates, the loading capacity on PCT increased as the MW of the polymer decreased, thus nCGO-PEG(2kDa) showed the highest loading of PCT around 67 %wt, while nCGO-PEG(20kDa) the lowest near 38 %wt. Probably, the almost 50 %wt decline in LC is associated with the extended polymeric chain of PEG(20kDa)-NH2 sterically hindering PCT loading, by obstructing the interaction with the nCGO lattice. The 4-arm PEG(10kDa)-NH_2 exhibited a PCT loading capacity of 33 %wt, lower than the 52 %wt loading of the linear PEG(10kDa)-NH_2.

The nCGO-PEG/PCT particles exhibited sustained slow PCT release at pH 7.4 with no burst effect (Figure 4A). Less than 40 % of the drug was released within the evaluated time period of 48 hours. The lowest release rate was shown by the nCGO-PEG(2kDa) around 30 %, while the high MW polymer particles showed similar release profiles. At pH 6.0 (Figure 4B) a higher PCT release was observed for all particles compared to the release at pH 7.4. The released PCT was almost 90 % at 48 hours for the nCGO-PEG(10kDa) particles, while the low MW nCGO-PEG(2kDa) had a release near to 60 %. In the case of nCGO-4armPEG(10kDa) particles burst effect is evidenced at pH 6.0, with a 50 % release in the first hour.

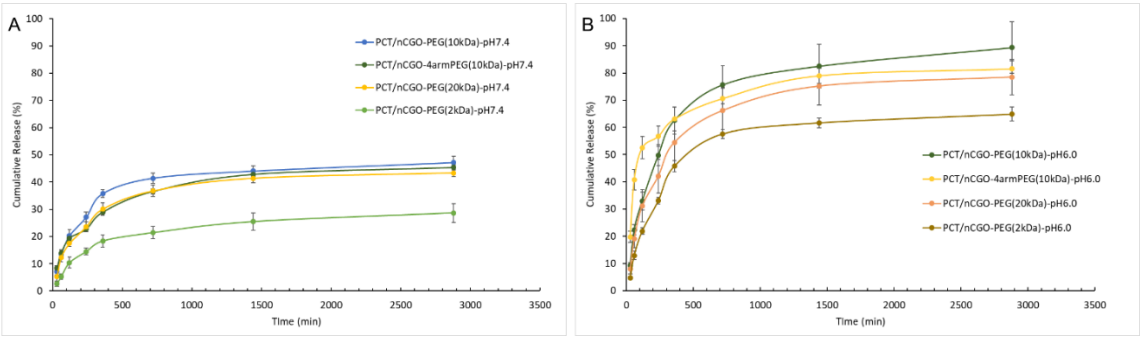

Figure 4. Paclitaxel release profile from the PCT/nCGO-PEG particles at PBS buffer of A) pH 7.4 and B) pH 6.0.

3.5. Results from the Cell Studies

For the in vitro cellular evaluation the nCGO-PEG(10kDa)/PCT particles was selected based on the colloidal stability results. Moreover, in a recent study by Khramtsov et al. [45] it was found that the type of PEG coating (branched or linear) affected the internalization of GO nanoparticles by cells and branched PEG-modified GO particles were less prompt to be internalized by cells than the linear-PEG modified ones, mainly due to the protein adsorption on the particles. Thus, the nCGO-PEG(10kDa)/PCT particles was opted for further study compared to the nCGO-4 arm PEG(10kDa)/PCT particles. Endocytosis is an important feature of graphene and graphene-based nanomedicine systems to effectively transport drug molecules within cellular compartments via receptor-mediated and non-specific mechanisms [1,46].

The cytotoxicity of nCGO-PEG(10kDa) against the A549 cell line was investigated at 5, 24 and 48 hours of incubation. The blank (no PCT) nCGO-PEG particles had lower cytotoxicity at all concentrations and incubation times than the blank nCGO particles (Figure 5), indicating an increased biocompatibility of the pegylated graphene oxide particles. Free PCT and nCGO-PEG(10kDa)/PCT particles exhibited comparable cytotoxicity at 5 hours of incubation that was close to 25 % at 25 μg/ml of PCT (Figure S8 of SI). At longer incubation time periods, the nCGO-PEG/PCT exhibited significantly ($p<0.01$) higher cytotoxicity compared to free PCT, reaching at the concentration of 25 μg/ml of PCT almost 60 % and 75 % cells destruction at 24 and 48 hours, respectively.

To further evaluate the in vitro anticancer activity of the nCGO-PEG/PCT particles their effect on cellular apoptosis was investigated. For this study, the nCGO (no PEG, no PCT) and the nCGO-PEG(10kDa) (no PCT) were evaluated as control samples and the effects of PCT and nCGO-PEG/PCT were compared with regard to the apoptotic damage induced in A549 cells. Figure 5 F shows that treatment of the cells with 10 μg/ml PCT and nCGO-PEG(10kDa)/PCT induced apoptosis in a time-dependent mode. The apoptosis level induced at 48 hours in the A549 cells by the nCGO, nCGO-

 doi:10.20944/preprints202410.1492.v1

PEG, PCT and nCGO-PEG/PCT particles were around 11±0.77 %, 8±0.72 %, 18±1.56 %, and 27±1.72 %, respectively. Moreover, the apoptosis analysis revealed that the PCT and nCGO-PEG/PCT reached a maximum of induced apoptosis at around 24 hours. The results showed that at all time-points the cell apoptosis was higher after nCGO-PEG/PCT treatment.

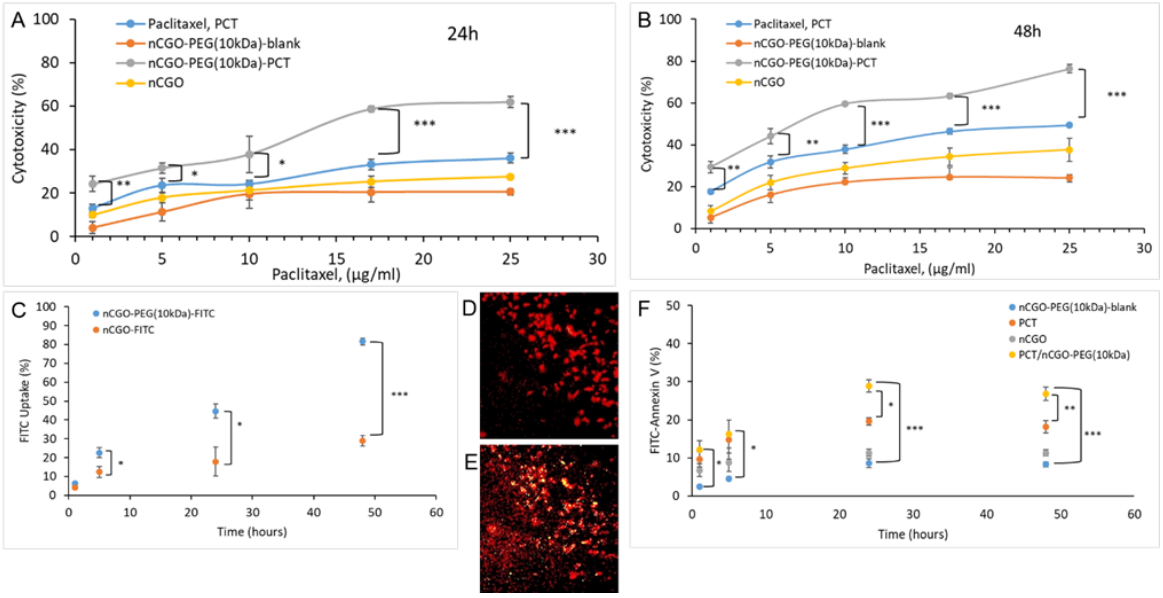

Figure 5. Cellular evaluation of the nCGO-PEG(10 kDa) particles against lung adenocarcinoma A549 cell line for the induced anticancer effect (cytotoxicity) at A) 24 hours (h) and B) 48 hours (h). C) Internalization of FITC-labelled nCGO-PEG(10kDa) in comparison with nCGO-particles and Fluorescence microscopy by PI post-fixation staining method of A549 cellular nuclei (D) and cells treated with FITC-labelled nCGO-PEG(10 kDa) particles (E). F) Evaluation on programmed cell death of A549 cells by apoptosis assay induced by nCGO (grey circles), nCGO-PEG(10 kDa) blank (na drug) (blue circles), PCT (orange circle), and nCGO-PEG(10 kDa)/PCT loaded (yellow circle) particles. The statistical significance is * $p < 0.01$, ** $p < 0.001$, *** $p < 0.0001$.

The internalization of nCGO and nCGO-PEG(10kDa) was evaluated quantitatively by FACS after labelling of the particles with FITC. Significant uptake with an almost linear increase with time was observed for the nCGO-PEG particles incubated with the A549 cells for 5, 24 and 48 hours (Figure 6C). The uptake of nCGO-PEG particles was significantly ($p < 0.01$) higher than that of nCGO particles at all times tested (Figure 5C). The post-fixation PI staining method was used to visualize the cellular uptake of the nCGO-PEG particles [21]. Under the experimental conditions used, PI can enter dead A549 cells (Figure 5D) and colocalize with FITC-labelled particles inside the cells to provide yellow colored areas (Figure 5E). Thus, the fluorescence microscopy images demonstrated the uptake of nCGO-PEG particles by the A549 cancer cells.

4. Discussion

Increased research interest has been devoted on the functionalization of GO family nanomaterials (including GO, rGO, and CGO) in order to optimize their therapeutic applications [45–50]. The advances effered by the modification of GO nanomaterials with PEG-based polymers has increased the prospects of their potential application in drug delivery and cancer therapeutics [51]. The synergistic effects of GO nanomaterials with chemotherapeutic agents, photodynamic /photothermal therapy, and sonotherapy represent a cutting edge field recently [52–54]. Shi et al. [52] reported the functionalization of rGO with PEG(5kDa) for the effective conjugation of TRC105 anti-CD105 antibody. A bifunctional succinimidyl carboxymethyl-PEG(5kDa)-maleimide (SCM-PEG-mal) polymer was used for the stabilization of nano rGO at a size range of 20 – 80 nm. Then, the PET isotope p-SCN-Bn-NOTA was effectively conjugated via a terminal amine linkage and the TRC105 antibody via Traut's reagent. The functionalized rGO expressed elevated photothermal properties

 doi:10.20944/preprints202410.1492.v1

and acted as a theranostic agent, by combining PET imaging and tumor vasculature CD105 targeting. Moreover, Guo et al. [53] studied the modification of GO with PEG(2 kDa)-bisNH_2 polymer through EDC/NHS chemistry for the conjugation of oxidized sodium alginate and the loading of Paclitaxel. The system showed pH/thermal-responsive drug release and was evaluated against Paclitaxel-resistant HGC-27 gastric cancer cells. Under, NIR-irradiation the GO system promoted elevated rate of apoptosis and mitochondrial damage of the HGC-27 cells, due to the combined photothermal/photodynamic effect of the GO lattice and anticancer effect of paclitaxel. In another study by Lee et al. [54], 4-arm PEG(2kDa)-NH_2 was used for the modification of GO and Graphene nanoribbons (GNR) for the delivery of the sonosensitizer chlorin e6 (Ce6). GNR-4arm PEG exhibited enhanced colloidal stability in cell culture media for up to 48 hours, while GO-4arm PEG was stable for up to 24 hours. In comparison GNR-4arm PEG expressed superior inhibition effects on tumor spheroids adhesion than GO-4arm PEG. Also, the GNR-4arm PEG system was evaluated on the inhibition and sonodynamic effect against ovarian cancer spheroids, resulting in reduced adhesion of the spheroids and reduced metastatic potential. Clearly, the binding affinity and biocompatibility of GO family nanomaterials can be significantly enhanced by PEG polymers' modification, reducing the tendency to aggregation, enhancing cytocompatibility effects, and regulating hemocompatibility [43,54]. In a recent study by Khramtsov et al. [47] it was highlighted that the polymeric chain of PEG (linear or branched) affected the surface serum protein adsorption on GO-PEG, due to diverse steric hindrance effects generated by the different polymeric chains. Moreover, the uptake of the GO-PEG nanoparticles from monocytes that were isolated from peripheral blood cells was affected, resulting in reduced internalization of the nanoparticles functionalized with branched PEG polymer.

In our study, we investigated the effect of PEG MW (relatively low = 2 kDa and relatively high = 10 and 20 kDa) and structure (linear or 4-arm branched PEG 10 kDa) on the basic physicochemical characteristics (Table 1), colloidal stability (Figure 2), hemocompatibility (Figure 3), and release of paclitaxel (Figure 4), of nCGO-PEG/PCT particles. Since, the modification of GO with linear or branched PEG has not been connected with differences in the observed cytotoxicity [45,47], the optimum nCGO-PEG/PCT particles was evaluated in cellular studies involving A549 lung adenocarcinoma cells (Figure 5).

The experimental process that was followed for the preparation of nCGO particles involved continuous steps of sonication / centrifugation / filtration, for the most stable aqueous nCGO suspension to be isolated. This process resulted in nCGO particles with a desired size of 76 nm and ζ-potential close to –48 mV that were further used for the conjugation of the various PEG-NH_2 polymers. Pegylation increased the size and ζ-potential of the particles (Table 1). An increase in the molecular weight of the (linear) PEG from 2 to 20 kDA decreased the size and tended to increase the ζ-potential of the nCGO-PEG particles (Table 1), indicating a more effective stabilizing and screening effect of the high MW PEG polymers. Also, a branched (4 arm) PEG(10 kDa) provided particles with significantly lower size and higher (less negative) ζ-potential compared to a linear PEG(10 kDa), probably as the result of a more effective coverage of graphene oxide surface by the branched polymer. Similar effects were observed by Liu et al. [55] which applied linear and branched PEG(40kDa) to stabilize nanoemulsions.

All nCGO-PEG particle types produced in this work, exhibited good colloidal stability on storage and in PBS and cell culture medium with the exception of the nCGO-PEG functionalized with the relatively low MW PEG of 2 kDa (Figure 2). Apparently, the relatively low molecular weight PEG chains of 2 kDa were unable to prevent a small degree of aggregation of the nCGO-PEG(2 kDa) particles. Pegylation decreased significantly the hemolytic potential of nCGO-PEG particles (Figure 3). All nCGO-PEG particles caused less than 5 % hemolysis even at a relatively high concentration of 1 mg/mL. This result, taken together with the lack of cytotoxicity of the nCGO-PEG particles (Figure 5), suggest the biocompatibility of nCGO-PEG although it is acknowledged that a more thorough biocompatibility study is required in order to fully appreciate the biocompatibility of the nCGO-PEG nanocarriers. The increased hemolytic potential of pristine nCGO (15 % at 1 mg/mL) is probably due to the electrostatic interactions of the RBCs with the plentiful oxygen groups of the nCGO surface. Moreover, the hydrophobic interactions between the pristine nCGO lattice and the phospholipids on

 doi:10.20944/preprints202410.1492.v1

the RBCs membrane may lead to the damage and disruption of the cellular membrane [43]. Pegylation increased the biocompatibility of graphene oxide particles by reducing the available oxygen molecules on the matrix and by offering a protective surface layer concealing the electrostatic interactions of oxygen molecules and the hydrophobic interactions of nCGO lattice with the RBCs.

For the delivery of PCT, non-covalent loading through physical adsorption was performed for all the nCGO-PEG particles, exploiting the π-π stacking interactions between the nCGO lattice and PCTs' aromatic rings [4,5]. An increase in PEG MW caused a decrease in PCT loading (Table 1), probably as a result of the more extensive steric hindrance of PCT adsorption on graphene oxide lattice by the longer PEG chains. A decrease in PCT loading capacity was observed with the 4 arm branched PEG(10kDa) compared to the linear PEG(10kDa) (Table 1). Khramtsov et al. [47], studied the effect of linear versus branched PEG polymers providing evidence that the branched-PEG shield the GO surface more effectively, due to their multiple chains that offer elevated steric hindrance. Thus, the lower PCT loading achieved with the nCGO-4armPEG conjugates can be attributed to the steric hindrance of the branched PEG(10kDa)-NH_2 polymeric chains affecting the adsorption of PCT on nCGO lattice. Support for this reasoning provides the relatively low PCT loading (11.2 %wt) reported by Xu et al. [46] for graphene oxide functionalized with a 6-armed poly(ethylene glycol). Zhuang et al. [45] conjugated carboxyl acid modified PCT on graphene oxide- 4 arm PEG-folic acid particles and succeeded an 18.7 % drug loading, thus the covalent PCT conjugation did not provide any improvement with regard to PCT loading on CGO.

At pH 7.4, slow drug release was observed from all the nCGO-PEG/PCT particles with less than 40 % PCT being released in 48 hours (Figure 4A). Low PCT leakage from the nanoparticles at physiological pH is necessary to avoid off target accumulation of drug before the nanoparticles reach the tumor area. Increased PCT release rate was observed at acidic pH 6.0 for all nCGO-PEG/PCT particles (Figure 4B). This may be because of the possibility of having stronger hydrogen bonding interaction between graphene oxide sheets and PCT at the basic conditions, resulting to lower PCT release rate [56]. The nCGO-PEG(2kDa) particles exhibited the lowest PCT release at both pH environments (Figure 4). The lower release rate of nCGO-PEG(2kDa) particles at both pH studied can probably be attributed to the reduced surface coverage provided by the relatively low MW polymeric chains of 2 kDa PEG. This allowed PCT to create strong π-π stacking and hydrophobic interactions with the graphite lattice. In the case of nCGO-4armPEG(10kDa) particles burst effect is evidenced at pH 6.0. In PEG branched polymers, PCT may also interact with the terminal active amine groups on the PEG branched chains through immobilization forming stable complexes [45]. At acidic pH such complexes may undergo hydrolysis at the N-terminal side facilitated by the hydroxyl groups of water that act as nucleophiles, leading to the degradation of the complexes and an initial elevated PCT release [48]. The increased drug release rate at acidic pH is a desirable attribute for anticancer particles since it can provide a more selective drug delivery at the acidic environment of tumors.

Among the various particles investigated, the nCGO-PEG(10kDa)/PCT exhibited optimal combination of properties including, average size (< 150 nm), colloidal stability, hemocompatibility, PCT loading, and release at pH 7.4 (< 40 %) and pH 6.0 (~90 %). Thus, the nCGO-PEG(10kDa)/PCT was selected for cellular studies. At 5 hours the nCGO-PEG/PCT and free PCT expressed comparable cytotoxicity values against the A549 cell line, while at 24 h and 48 h the nCGO-PEG(10kDa)/PCT significantly surpassed the anticancer activity of free PCT (Figure 5A, B). Specifically, the IC50 at 48 hours of nCGO-PEG(10kDa)/PCT was near 5 μg/ml of drug, while free PCT showed IC50 near 25 μg/ml. The higher cytotoxicity of the particles-entrapped PCT compared to free PCT at higher incubation times may be attributed to the increasing with time cellular uptake of nanoparticles (Figure 5C). The cytotoxicity of nCGO-PEG(10kDa)/PCT reached at the concentration of 25 μg/ml on a PCT basis 60% and 75 % cells destruction at 24 and 48 hours, respectively. A little lower cytotoxicity against the A549 cell line has been reported for nano GO particles stabilized with PLA-PEG copolymers [13]. The effect of PCT-loaded, 6-armed PEG-functionalized graphene oxide particles on the viability of A549 cells has been investigated by Xu et al. [46] that showed significantly increased cell death close to 70 % at 1.29 mg/L particles concentration. In a more recent study by Lin et al. [49], graphene oxide was reduced with *Euphorbia milii* leaves extract and then was loaded with PCT. The

 doi:10.20944/preprints202410.1492.v1

reduced graphene oxide/Paclitaxel complexes, showed a dose-dependent reduction in A549 cells viability that reached 10 % at the concentration of 500 μg/mL after a 24 hours' incubation period.

To further investigate the anticancer ability of nCGO-PEG/PCT particles in relation to free PCT, the apoptotic effect against A549 cells was examined (Figure 5F). The results supported increased presence of apoptotic cells, expressed at 24 and 48 hours, by the nCGO-PEG/PCT particles, reaching a maximum at 24 h post-incubation. In a recent study by Zhao et al. [34] the antitumor effect and the mechanism of induced apoptosis of Paclitaxel and Paclitaxel-nanoparticles on A549 cells was investigated. The evaluation concluded that the Paclitaxel-NP significantly inhibited the G2 phase of cell cycle and increased programmed cell death. The outmost of the effect on G2 phase and cellular apoptosis was observed at 15 hours after light onset (HALO). The effect of PEG modification on the induced apoptosis was the nCGO-PEG particles to cause less than 10 % of programmed cell death at 48 hours, while a slightly increased apoptosis rate was induced by the nCGO control samples. The effect of PEG modification on cellular uptake was also evaluated (Figure 5C). The nCGO control samples expressed significantly reduced uptake rate in comparison to the nCGO-PEG especially at 24 and 48 hours, suggesting the elevated tumor cell accumulation ability provided by the functionalization of nCGO nanosheets with PEG [4,5].

5. Conclusions

This section is not mandatory but can be added to the manuscript if the discussion is unusually long or complex. Based on the results obtained in this study, pegylation of CGO nanoparticles significantly improved the biocompatibility aspects of the particles, as evidenced by the reduced hemolytic potential and decreased cytotoxicity of the pegylated particles. The characteristics (molecular weight and structure) of PEG significantly affected the physicochemical and drug release properties of the pegylated CGO nanoparticles. The nCGO-PEG/PCT nanoparticles exhibited pH sensitive drug release properties, having a significantly higher drug release at pH 6.0 compared to the physiological pH. The latter is a desirable attribute for antitumor particles. The pegylated CGO nanoparticles exhibited high uptake by the A 549 cancer cell line, which led to a strong anticancer activity upon incubation of the nCGO-PEG/PCT nanoparticles with the A549 cells. The obtained results justify further investigation of the potential of nCGO-PEG/PCT for effective destruction of tumors in vivo.

Supplementary Materials: The following supporting information can be downloaded at: www.mdpi.com/xxx/s1. The SI material published online alongside the article concerns the details for the successful synthesis and characterization of GO and CGO, and supporting figures as follows, Figure S1: XRD pattern of graphite (black line), GO (purple line) and CGO (green line). Figure S2: FTIR spectra of graphite (black line), GO (purple line) and CGO (green line). Figure S3: Raman spectra of graphite (black line), GO (purple line) and CGO (green line). Figure S4: 1H NMR Spectra of A) nCGO formulations, B) PEG (10 kDa) -NH2 polymer, C) nCGO-PEG(10 kDa) formulations in D2O. Figure S5: TGA of nCGO-PEG formulations (blue line) in comparison with the specific mPEG-NH2 polymer (red line) and nCGO (black line). Figure S6: TEM micrographs of nCGO (A), nCGO-PEG(2 kDa) (B), nCGO-PEG(20 kDa) (C), and nCGO-4 arm PEG(10 kDa). Figure S7: Colloidal stability of nCGO and nCGO-PEG formulations in biological media (RPMI 1640, and PBS). Average variations of A) main peak by DLS and B) PDI Figure S8: Cytotoxicity of nCGO-PEG(10 kDa) against A549 cancer cells at 5 hours (h) of incubation.

Author Contributions: Conceptualization, Dimitrios Gournis and and Konstantinos Avgoustakis; Data curation, Athina Angelopoulou; Formal analysis, Athina Angelopoulou; Investigation, Athina Angelopoulou, Myria Papachristodoulou, Efstathia Voulgari, Andreas Mouikis and Panagiota Zygouri; Methodology, Athina Angelopoulou, Myria Papachristodoulou, Efstathia Voulgari, Andreas Mouikis and Panagiota Zygouri; Supervision, and Konstantinos Avgoustakis; Validation, Athina Angelopoulou, Myria Papachristodoulou, Efstathia Voulgari and Andreas Mouikis; Visualization, Dimitrios Gournis and and Konstantinos Avgoustakis; Writing – original draft, Athina Angelopoulou; Writing – review & editing, Athina Angelopoulou, Panagiota Zygouri, Dimitrios Gournis and and Konstantinos Avgoustakis. All authors have read and agreed to the published version of the manuscript.

Funding: This research received no external funding.

Acknowledgments: The authors thank the Lab of Electron Microscopy and Microanalysis at the University of Patras for the TEM images.

Conflicts of Interest: The authors declare no conflicts of interest.

References

1. Shafiee, A.; Iravani, S.; Varna, R.S. Graphene and graphene oxide with anticancer applications: Challenges and future perspectives. MedComm. 2022, 3, e118. https://doi.org/10.1002/mco2.118
2. Mohd Itoo, A.; Lakshmi Vemula, S.; Tejasvni Gupta, M.; Vilasrao Giram, M.; Akhil Kumar, S.; Ghosh, B.; Biswas. S. Multifunctional graphene oxide nanoparticles for drug delivery in cancer. J. Contr. Rel. 2022, 350, 26. https://doi.org/10.1016/j.jconrel.2022.08.011
3. de Melo-Diogo, D.; Lita-Sousa, R.; Alves, C.G.; Costa, E.C.; Louro, R.O.; Correia. I.J. Functionalization of graphene family nanomaterials for application in cancer therapy. Colloids Surf. B Biointerfaces. 2018, 171, 260. https://doi.org/10.1016/j.colsurfb.2018.07.030
4. Alemi, F.; Zarezadeh, R.; Raei Sadigh, A.; Hamishehkar, H.; Rahimi, M.; Majidinia, M.; Asemi, Z.; Ebrahimi-Kalan, A.; Yousefi, B.; Rashtchizadeh. N. Graphene oxide and reduced graphene oxide: Efficient cargo platforms for cancer theranostics. J. Drug Deliev. Sci. & Techn. 2020, 60, 101974. https://doi.org/10.1016/j.jddst.2020.101974
5. de Melo-Diogo, D.; Lita-Sousa, R.; Alves, C.G.; Correia, I.J. Graphene family nanomaterials for application in cancer combination photothermal therapy. Biomater. Sci., 2019, 7, 3534. https://doi.org/10.1039/C9BM00577C
6. Yang, K.; Zhang, S.; Zhang, G.; Sun, X.; Lee, S.-T.; Liu, Z. Graphene in mice: ultrahigh in vivo tumor uptake and efficient photothermal therapy. Nano Lett., 2010, 10, 3318. https://doi.org/10.1021/nl100996u
7. Li, Y.; Feng, L.; Shi, X.; Wang, X.; Yang, Y.; Yang, K.; Liu, T.; Yang, G.; Liu, Z. Surface coating-dependent cytotoxicity and degradation of graphene derivatives: towards the design of Non-toxic, degradable nano-graphene. Small, 2014, 10, 1544. https://doi.org/10.1002/smll.201303234
8. Zhang, S.; Yang, K.; Feng, L.; Liu, Z. In vitro and in vivo behaviors of dextran functionalized graphene. Carbon, 2011, 49, 4040. https://doi.org/10.1016/j.carbon.2011.05.056
9. Cheng, C.; Li, S.; Nie, S.; Zhao, W.; Yang, H.; Sun, S.; Zhao, C. General and biomimetic approach to biopolymer-functionalized graphene oxide nanosheet through adhesive dopamine. Biomacromolecules, 2012, 13, 4236. https://doi.org/10.1021/bm3014999
10. Rana, V.K.; Choi, M.-C.; Kong, J.-Y.; Kim, G.Y.; Kim, M.J.; Kim, S.-H.; Mishra, S.; Singh, R.P.; Ha, C.-S. Synthesis and drug-delivery behavior of chitosan-functionalized graphene oxide hybrid nanosheets. Macromol. Mater. Eng., 2011, 296, 131. https://doi.org/10.1002/mame.201000307
11. Xu, M.; Zhu, J.; Wang, F.; Xiong, Y.; Wu, Y.; Wang, Q.; Weng, J.; Zhang, Z.; Chen, W.; Liu, S. Improved in vitro and in vivo biocompatibility of graphene oxide through surface modification: poly(acrylic acid)-functionalization is superior to PEGylation. ACS Nano, 2016, 10, 3267. https://doi.org/10.1021/acsnano.6b00539
12. Yang, K.; Wan, J.; Zhang, S.; Tian, B.; Zhang, Y.; Liu, Z. The influence of surface chemistry and size of nanoscale graphene oxide on photothermal therapy of cancer using ultra-low laser power. Biomaterials, 2012, 33, 2206. https://doi.org/10.1016/j.biomaterials.2011.11.064
13. Angelopoulou, A.; Voulgari, E.; Diamanti, E.K.; Gournis, D.; Avgoustakis, K. Graphene oxide stabilized by PLA–PEG copolymers for the controlled delivery of paclitaxel. Eur. J. Pharm. Biopharm. 2015, 93, 18. https://doi.org/10.1016/j.ejpb.2015.03.022
14. Alibolandi, M.; Mohammadi, M.; Taghdisi, S.M.; Ramezani, M.; Abnous, K. Fabrication of aptamer decorated dextran coated nano-graphene oxide for targeted drug delivery. Carbohydr. Polym., 2017, 155, 218. https://doi.org/10.1016/j.carbpol.2016.08.046
15. Hong, B.J.; Compton, O.C.; An, Z.; Eryazici, I.; Nguyen, S.T. Successful stabilization of graphene oxide in electrolyte solutions: enhancement of biofunctionalization and cellular uptake. ACS Nano, 2012, 6, 63. https://doi.org/10.1021/nn202355p
16. de Melo-Diogo, D.; Pais-Silva, C.; Costa, E.C.; Louro, R.O.; Correia, I.J. D-α-tocopheryl polyethylene glycol 1000 succinate functionalized nanographene oxide for cancer therapy. Nanomedicine, 2017, 12, 443. https://doi.org/10.2217/nnm-2016-0384

17. Li, R.; Wang, Y.; Du, J.; Wang, X.; Duan, A.; Gao, R.; Liu, J;. Li, B. Graphene oxide loaded with tumor-targeted peptide and anti-cancer drugs for cancer target therapy. Sci Rep. 2021, 11, 1725. https://doi.org/10.1038/s41598-021-81218-3
18. Vinothini, K.; Rajendran, N.K.; Ramu, A.; Elumalai, n.; Rajan, M. Folate receptor targeted delivery of paclitaxel to breast cancer cells via folic acid conjugated graphene oxide grafted methyl acrylate nanocarrier. Biomed. & Pharmacother. 2019, 110, 906. https://doi.org/10.1016/j.biopha.2018.12.008
19. Samadian, H.; Mohammad-Razaei, R.; Jahanban-Esfahlan, R.; Massoumi, B.; Abbasian, M.; Jafarizad, A.; Jaymand, M. A de novo theranostic nanomedicine composed of PEGylated graphene oxide and gold nanoparticles for cancer therapy. J. Mater. Res. 2020, 35, 430. https://doi.org/10.1557/jmr.2020.3
20. Hussien, N.A.; Isiklan, N.; Turk, M. Aptamer-functionalized magnetic graphene oxide nanocarrier for targeted drug delivery of paclitaxel. Mater. Chem. Physic. 2018, 211, 479. https://doi.org/10.1016/j.matchemphys.2018.03.015
21. Yaghoubi, F.; Morteza Naghib, S.; Hosseini Motlagh, N.S.; Haghiralsadat, F.; Zarei Jaliani, H.; Moradi, A. Multiresponsive carboxylated graphene oxide grafted aptamer as a multifunctional nanocarrier for targeted delivery of chemotherapeutics and bioactive compounds in cancer therapy. Nanotech. Rev. 2021, 10, 1838. https://doi.org/10.1515/ntrev-2021-0110
22. Jedrzejczak-Silicka, M.; urbas, K.; Mijowska, E.; Rakoczy, R. The covalent and non-covalent conjugation of graphene oxide with hydroxycamptothecin in hyperthermia for its anticancer activity. J. Alloys Compd. 2017, 709, 112. http://dx.doi.org/10.1016/j.jallcom.2017.03.146
23. Sharma, H.; Mondal, S. Functionalized Graphene Oxide for Chemotherapeutic Drug Delivery and Cancer Treatment: A Promising Material in Nanomedicine. Int. J. Mol. Sci. 2020, 21, 6280. https://doi.org/10.3390/ijms21176280
24. Song, S.; Shen, H.; Wang, Y.; Chu, X.; Xie, J.; Zhou, N.; Shen, J. Biomedical application of graphene: From drug delivery, tumor therapy, to theranostics. Colloids Surf B Biointerfaces. 2020, 185, 110596. https://doi.org/10.1016/j.colsurfb.2019.110596
25. Zhao, H.; Ding, R.; Zhao, X.; Li, Y.; Qu, L.; Pei, H.; Yildirimer, L.; Wu, Z.; Zhang W. Graphene-based nanomaterials for drug and/or gene delivery, bioimaging, and tissue engineering. Drug Discov. Today. 2017, 22, 1302. https://doi.org/10.1016/j.drudis.2017.04.002
26. Amiryaghoubi, N.; Fathi, M.; Barzegari, A.; Barar, J.; Omidian, H.; Omidi, Y. Recent advances in polymeric scaffolds containing carbon nanotube and graphene oxide for cartilage and bone regeneration. Mater. Today Commun. 2021, 26, 102097. https://doi.org/10.1016/j.mtcomm.2021.102097
27. Eltaweil, A.S.; Ahmed M. S.; El-Subruiti, G.M.; Khalifa, R. E.; Omer, A. M. Efficient loading and delivery of ciprofloxacin by smart alginate/carboxylated graphene oxide/aminated chitosan composite microbeads: In vitro release and kinetic studies. Arab. J. Chem., 2023, 16, 104533, https://doi.org/10.1016/j.arabjc.2022.104533
28. Gholami, A.; Emadi, F.; Nazem, M.; Aghayi, R.; Khalvati, B.; Amini A.; Ghasemi., Y. Expression of key apoptotic genes in hepatocellular carcinoma cell line treated with etoposide-loaded graphene oxide. J Drug Delivery Sci Technol. 2020, 57, 101725. https://doi.org/10.1016/j.jddst.2020.101725
29. Spyrou, K.; Calvaresi, M.; Diamanti, E.K.; Tsoufis, T.; Gournis, D.; Rudolf, P.; Zerbetto, F. Graphite Oxide and Aromatic Amines: Size Matters. Adv. Funct. Mater. 2015, 25, 263. https://doi.org/10.1002/adfm.201402622
30. Zygouri, P.; Spyrou, K.; Papayannis, D.K.; Asimakopoulos, G.; Dounousi, E.; Stamatis, H.; Gournis, D.; Rudolf, P. Comparative Study of Various Graphene Oxide Structures as Efficient Drug Release Systems for Ibuprofen. Applied. Chem. 2022, 2, 93. https://doi.org/10.3390/appliedchem2020006
31. Farooq, S.; Aziz, H.; Ali, S.; Murtaza, G.; Rizwan, M.; Saleem, M.H.; Mahboob, S.; Al-Ghanim, K.A.; Riaz, M.N.; Murtaza, B. Synthesis of Functionalized Carboxylated Graphene Oxide for the Remediation of Pb and Cr Contaminated Water. Int. J. Environ. Res. Public Health 2022, 19, 10610. https://doi.org/10.3390/ijerph191710610
32. Angelopoulou, A.; Kolokithas-Ntoukas, A.; Papaioannou, L.; Kakazanis, Z.; Khoury, N.; Zoumpourlis, V.; Papatheodorou, S.; Kardamakis, D., Bakandritsos, A.; Hatziantoniou, S.; Avgoustakis. K. Canagliflozin-loaded magnetic nanoparticles as potential treatment of hypoxic tumors in combination with radiotherapy, Nanomedicine. 2018, 13, 1. https://doi.org/10.2217/nnm-2018-0145

33. Georgitsopoulou, S.; Angelopoulou, A.; Papaioannou, L.; Georgakilas, V.; Avgoustakis. K. Self-assembled Janus graphene nanostructures with high camptothecin loading for increased cytotoxicity to cancer cells. J. Drug Deliv. Sci. Technol. 2022, 6, 102971. https://doi.org/10.1016/j.jddst.2021.102971
34. Zhao, X.; Fuan, J.; Wu, P.; Wei, C.; Chen, Q.; Ming, Z.; Yan, J.; Yang, L. Chronic chemotherapy with paclitaxel nanoparticles induced apoptosis in lung cancer in vitro and in vivo. Int. J. Nanomed. 2019, 14, 1299, http://dx.doi.org/10.2147/IJN.S188049
35. Hezel, M.; Ebrahimi, F.; Koch, M.; Dehghani, F. Propidium iodide staining: a new application in fluorescence microscopy for analysis of cytoarchitecture in adult and developing rodent brain, Micron. 2012, 43 1031. https://doi.org/10.1016/j.micron.2012.04.006
36. Ambrozio, A.R.; Lopes, T.R.; Cipriano, D.F.; de Souza F.A.L.; Scopel, W.L.; Freitas, J.C.C. Combined experimental and computational 1H NMR study of water adsorption onto graphenic materials. JMRO. 2023, 14, 100091. https://doi.org/10.1016/j.jmro.2022.100091
37. Bichenkova, E.V.; Raju, A.P.A.; Burusco, K.K.; Kinloch, I.A.; Novoselov, K.S.; Clarke, D.J. NMR detects molecular interactions of graphene with aromatic and aliphatic hydrocarbons in water. 2D Mater. 2018, 5, 015003. https://doi.org/10.1088/2053-1583/aa8abe
38. Mobin, M.; Huda; Shoeb, M.; Aslam, R.; Banerjee, P. Synthesis, characterisation and corrosion inhibition assessment of a novel ionic liquid-graphene oxide nanohybrid. J. Mol. Struct. 2022, 1262, 133027. https://doi.org/10.1016/j.molstruc.2022.133027
39. Depan, D.; Shah, J.; Misra, R.D.K. Controlled release of drug from folate-decorated and graphene mediated drug delivery system: Synthesis, loading efficiency, and drug release response. Mater. Sci. Eng. C. 2011, 31, 1305. https://doi.org/10.1016/j.msec.2011.04.010
40. Sam, S.; Touahir, L.; Salvador Andresa, J.; Allongue, P.; Chazalviel, J.-N.; Gouget-Laemmel, A.C.; de Villeneuve, C.H.; Moraillon, A.; Ozanam, F.; Gabouze, N.; Djebbar, S. Semiquantitative Study of the EDC/NHS Activation of Acid Terminal Groups at Modified Porous Silicon Surfaces, Langmuir. 2010, 26, 809. https://doi.org/10.1021/la902220a
41. Shariare, M.H.; Masum, A.-A.; Alshehri, S.; Alanazi, F.K.; Uddin, J.; Kazi, M. Preparation and Optimization of PEGylated Nano Graphene Oxide-Based Delivery System for Drugs with Different Molecular Structures Using Design of Experiment (DoE). Molecules. 2021, 26, 1457. https://doi.org/10.3390/molecules26051457
42. Ramezani Farani, M.; Khadiv-Parsi, P.; Hossein Riazi, G.; Shafiee Ardestani, M.; Saligheh Rad, H. PEGylation of graphene/iron oxide nanocomposite: assessment of release of doxorubicin, magnetically targeted drug delivery and photothermal therapy. Appl. Nanosci. 2020, 10, 1205. https://doi.org/10.1007/s13204-020-01255-8
43. Kamenska, T.; Abrashev, M.; Georgieva, M.; Krasteva, N. Impact of Polyethylene Glycol Functionalization of Graphene Oxide on Anticoagulation and Haemolytic Properties of Human Blood. Materials 2021, 14, 4853. https://doi.org/10.3390/ma14174853
44. Hashemzadeh, H.; Raissi, H. Understanding loading, diffusion and releasing of Doxorubicin and Paclitaxel dual delivery in graphene and graphene oxide carriers as highly efficient drug delivery systems. Applied Surf. Sci. 2020, 500, 144220. https://doi.org/10.1016/j.apsusc.2019.144220
45. Zhuang, W.; He, L.; Wang, K.; Ma, B.; Ge, L.; Wang, Z.; Huang, J.; Wu, J.; Zhang, Q.; Ying, H. Combined Adsorption and Covalent Linking of Paclitaxel on Functionalized Nano-Graphene Oxide for Inhibiting Cancer Cells. ACS Omega 2018, 3, 2396. https://doi.org/10.1021/acsomega.7b02022
46. Xu, Z.; Wang, S.; Li, Y.; Wang, M.; Shi, P.; Huang, X. Covalent Functionalization of Graphene Oxide with Biocompatible Poly(ethylene glycol) for Delivery of Paclitaxel. ACS Appl. Mater. Interfaces. 2014, 6, 19, 17268. https://doi.org/10.1021/am505308f
47. Khramtsov, P.; Bochkova, M.; Timganova, V.; Nechaev, A.; Uzhviyuk, S.; Shardina, K.; Maslennikova, I.; Rayev, M.; Zamorina, S. Interaction of Graphene Oxide Modified with Linear and Branched PEG with Monocytes Isolated from Human Blood. Nanomaterials. 2022, 12, 126. https://doi.org/10.3390/nano12010126
48. Rodrigues, R.C.; Berenguer-Murcia, A.; Carballares, D.; Morellon-Sterling, R.; Fernandez-Lafuente, R. Stabilization of enzymes via immobilization: Multipoint covalent attachment and other stabilization strategies. Biotech. Adv. 2021, 52, 107821. https://doi.org/10.1016/j.biotechadv.2021.107821
49. Lin, S.; Ruan, J.; Wang, S. Biosynthesized of reduced graphene oxide nanosheets and its loading with paclitaxel for their anti-cancer effect for treatment of lung cancer. J. Photochem. Photobiol. B: Biology. 2019, 191, 13. https://doi.org/10.1016/j.jphotobiol.2018.11.015

 doi:10.20944/preprints202410.1492.v1

50. Sari, M.M. Fluorescein isothiocyanate conjugated graphene oxide for detection of dopamine, Mater. Chem. Phys. 2013, 138, 843. https://doi.org/10.1016/j.matchemphys.2012.12.069
51. Sell, M.; Lopes, A.R.; Escudeiro, M.; Esteves, B.; Monteiro, A.R.; Trindade, T.; Cruz-Lopes, L. Application of Nanoparticles in Cancer Treatment: A Concise Review. Nanomaterials. 2023, 13, 2887. https://doi.org/10.3390/nano13212887
52. Shi, S.; Yang, K.; Hong, H.; Valdovinos, H.F.; Nayak, T.R.; Zhang, Y.; Theuer, C.P.; Barnhart, T.E.; Liu, Z.; Cai, W. Tumor vasculature targeting and imaging in living mice with reduced graphene oxide, Biomaterials. 2013, 34, 3002. https://doi.org/10.1016/j.biomaterials.2013.01.047
53. Guo, W.; Chen, Z.; Feng, X.; Shen, G.; Huang, H.; Liang, Y.; Zhao, B.; Li, G.; Hu, Y. Graphene oxide (GO)-based nanosheets with combined chemo/photothermal/ photodynamic therapy to overcome gastric cancer (GC) paclitaxel resistance by reducing mitochondria-derived adenosine-triphosphate (ATP). J Nanobiotechnol. 2021, 19, 146. https://doi.org/10.1186/s12951-021-00874-9
54. Lee, H. R.; Kim, D. W.; Jones, V. O.; Choi, Y.; Ferry, V. E.; Geller, M. A.; Azarin, S. M. Sonosensitizer-Functionalized Graphene Nanoribbons for Adhesion Blocking and Sonodynamic Ablation of Ovarian Cancer Spheroids. Adv. Healthcare Mater. 2021, 10, 2001368. https://doi.org/10.1002/adhm.202001368
55. Liu, M.; Zhao, D.; Yan, N.; Li, J.; Zhang, H.; Liu, M.; Tang, X.; Liu, X.; Deng, Y.; Song, Y.; Zhao, X. Evasion of the accelerated blood clearance phenomenon by branched PEG lipid derivative coating of nanoemulsions, Int. J. Pharm. 2022, 612, 121365. https://doi.org/10.1016/j.ijpharm.2021.121365
56. Awel Hussien, N.; Işıklan, N.; Türk, M. Aptamer-functionalized magnetic graphene oxide nanocarrier for targeted drug delivery of paclitaxel, Mater. Chem. Phys. 2018, 211, 479. https://doi.org/10.1016/j.matchemphys.2018.03.015